Comparing Data and Predictions for TeV Candidate BL Lacs

Elizabeth Hays and Julie McEnery

December 18, 2003

1 Intro

In a paper by Costamante and Ghisellini GeV/TeV flux predictions are given for a group of BL Lacs selected as TeV candidates (astro-ph/0112201) [4]. The candidates that fall within the field-of-view of Milagro are the subjects of a search in 2.5 years of Milagro data. None of the BL Lacs are detected in this data set. However, for several sources the upper limits on the flux fall below the predictions given by Costamante and Ghisellini. Their predictions do not include any type of cut-off in the energy spectrum such as that due to attenuation of photons by infrared background light. The presence of a cut off is one possible explanation for the constrained fluxes.

Separate limits are presented for two spectra chosen independently of the Costamante and Ghisellini predictions to provide a range for the results. These limits are also given with IR attenuation effects included. A limit including a spectral energy cut off is necessary because cut offs are observed in AGN detected at TeV energies [Samuelson et al.(1998)] [Krennrich et al.(1999)] [Aharonian et al.(1999)] [Aharonian et al.(2002)]. The limits presented this way relate more closely to source emission than to IR attenuation. In this memo I outline the predictions made by Costamante and Ghisellini and report the limits from Milagro data calculated for several spectral shapes.

2 TeV Candidate BL Lacs

In Costamante and Ghisellini (2002) [4] a sample of BL Lacs are selected as favorable sources of TeV emission based on brightness in x-ray and radio surveys. Costamante and Ghisellini argue that in this range the electron population and seed photon population contributing to the highest energy

photon emission are maximized. Previously observed TeV emitting BL Lacs, Mrk 501, Mrk 421, H 1426+428, 1ES 2344 and PKS 2155-304 fall within this parameter space and one of the selected sample, 1ES 1959+650, has since been detected by air-Čerenkov telescopes. The criteria chosen by Costamante and Ghisellini select thirty-two objects from several BL Lac samples as the best TeV candidates. Of this set twenty-seven fall within the field of view of Milagro which is about 0° to 80° DEC for transiting sources.

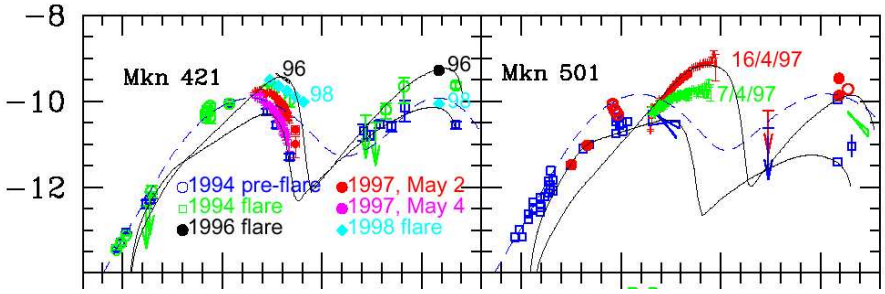

Figure 1: Extreme blazar spectral energy density (SED) fits to Mrk 421 and Mrk501 radio, optical and x-ray data [4]. The solid lines are SSC fits and the dotted line is the modified Fossati model fit. The y axis is log νF_ν in ergs/cm^2 s. The x axis is log frequency in Hz from 10^8 to 10^{28} Hz.

Costamante and Ghisellini use optical, radio, and x-ray data for each candidate to fit the spectral energy density (SED) and then make predictions for the integral flux above GeV and TeV energies. Two types of models are applied to fit the SEDs (Figure 1). The first is the phenomenological model of Fossati [5] with modifications by Donato and Costamante for low power BL Lacs. The Fossati parameterization predicts the location of the inverse Compton (IC) peak and relation of IC to synchrotron luminosity using the blazar sequence. The parameterization is based on observations that blazars with larger radio luminosity have progressively higher frequency synchrotron and IC peaks and lower IC luminosity. The SED peaks are fit using parabolic forms in this model. The second model is an homogeneous, one-zone synchrotron self-Compton (SSC) model with a finite time electron injection. This assumes a small emission region of synchrotron emitting electrons. The finite time injection allows electrons to have a characteristic cooling time that steepens the electron energy spectrum at the high energies. The SSC model predicts less emission at TeV energies to the energy dependence of the IC cross section at very high energies. Both models are used to predict an SED that is used to obtain integral fluxes above 40 GeV, 300 GeV and 1 TeV.

3 Discussion of Milagro Flux Limits

For purposes of the memo this section attempts some general interpretations of flux results from Milagro data that can be applied to the given results. Because Milagro has sensitivity over a broad energy range without energy resolution, the calculation of flux from Milagro data depends on the assumed energy spectrum. The shape of the energy spectrum can take many forms, but for simplicity a power law is assumed, optionally with an energy dependent attenuation or an exponential energy cut off.

$$\frac{dN}{dE} \propto E^{-\alpha} e^{-\tau(E,z)} \tag{1}$$

or

$$\frac{dN}{dE} \propto E^{-\alpha} \exp^{-E/E_c} \tag{2}$$

The energy at which Milagro is most sensitive to a source depends on the shape of the assumed energy spectrum. In the case of a Crab spectrum with no cut off, where $dN/dE = I_0 E^{-2.49}$, the energy at which the differential flux is least sensitive to changes in the spectral shape is the median triggered energy, about 4 TeV. In the case of a source affected by an energy cut off there may be no detectable emission above 1 TeV. The median energy for the Crab spectrum would seem to imply that Milagro would have no sensitivity to the source. However, Milagro still has effective area at energies below 1 TeV. This allows detection of photons at energies below the cut-off energy even though Milagro has less sensitivity there. In this case, the energy at which Milagro is most sensitive to that source will be the cut-off energy. This means that the same observation can produce different flux limits at different energies depending on the assumed spectrum, particularly in the case of a cut off in the spectrum.

The calculation of flux from the photon rate in Milagro data assumes a spectral shape. The calculation takes the background subtracted event rate at the source position and finds the factor that makes the photon rate for an assumed photon spectrum combined with Milagro's detection efficiency for the path of the source over the time period and energy range of the observation match the observed rate . Changing the spectral shape requires the factor, I_0, to change to compensate for the assumed energy distribution of photons. The dependence of I_0 on the elements of spectral shape, power law index and energy dependent attenuation is not straightforward because

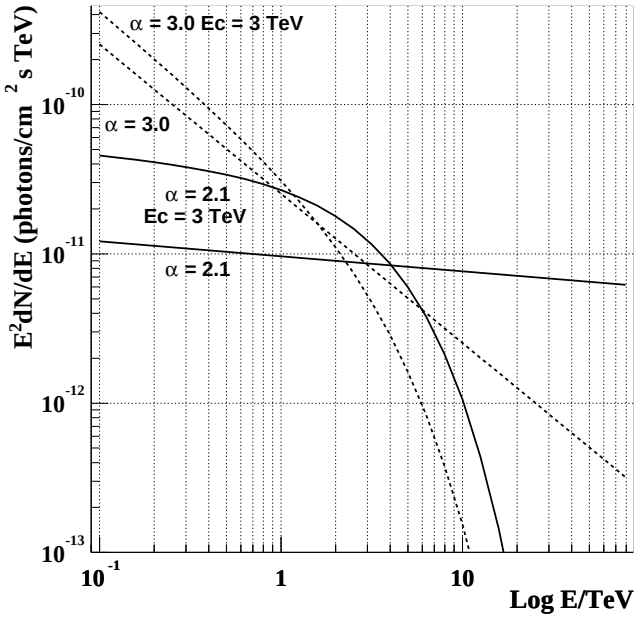

Figure 2: Differential flux dependence on an assumed spectral shape. The plot shows $E^2 dN/dE$ where $dN/dE = I_0(E/TeV)^{-\alpha} e^{-E/E_c}$ or in the case of no cut-off energy $dN/dE = I_0(E/TeV)^{-\alpha}$. For each curve the event rate in the detector is the same and the differential flux is calculated for the assumed values of α and cut-off energy, E_c. The values of I_0 for each combination are given in Table 1.

Milagro has energy sensitivity above and below an energy cut off. When interpreting the dependence of I_0 on the IR models both the cut off and spectral index must be considered. To give a better idea of how the limit depends on the choice of spectrum, E^2dN/dE is plotted assuming several spectral shapes. For each shape I_0 is calculated for the same observed count rate in the detector. I_0 determines the "height" of the spectrum on this plot. Table 1 lists the calculated I_0 for each spectral shape with the median triggered energy for that spectrum and the integrated flux above the median energy.

α	E_c (TeV)	I_o ($10^{-11}\frac{phot}{cm^2 s TeV}$)	E_{med} (TeV)	$F > E_{med}$ ($10^{-12}\frac{phot}{cm^2 s}$)
2.1	none	0.96	6.31	1.09
2.1	3	3.73	1.74	4.59
3.0	none	2.53	1.32	7.26
3.0	3	4.31	0.72	24.69

Table 1: Related numbers for Figure 2 of $E^2 dN/dE$ where $dN/dE = I_o E^{-\alpha} e^{-E/Ec}$. The differential flux factor, I_0, is calculated for an event rate of 10 phot/day from a source with the given energy spectrum at declination 26°. The median triggered energy and the integral flux above the median triggered energy are also given.

4 Inclusion of Infra-red Background Attenuation

The extragalactic Infra-red (IR) background is expected to have an observable impact on the spectra of AGN at TeV energies. Current AGN observations at TeV energies show strong evidence for a cut off. It is common practice to present AGN results with IR absorption effects removed from the spectrum to give a better idea of the flux at the source. In the case of Milagro, the assumed spectrum must be modified to include energy dependent attenuation. This causes the calculated flux to include that lost by attenuation and represent the emission at the source as opposed to at the Earth.

Several approaches have been taken to predicting the luminosity of extragalactic background light. For the purposes of this memo, the model of Stecker and de Jager (2001) [9], which predicts the absorption parameterized in energy and redshift, is used for ease of application to sources at a variety of redshifts. Many of the AGN in the sample have a measured redshift. For those that do not have a measured redshift, the mean of the Costamante and Ghisellini (2001) BL Lac sample, $z = 0.2$, is used. The predicted optical depth from the model is applied to an assumed differential spectrum of the form of Equation (1). The attenuated spectrum is then used in the flux calculation to obtain the flux at the source. For further details see memo (6-19-2003).

5 Milagro DC Dataset

The data set used for this analysis begins on Dec. 15, 2000 and ends on June 12, 2003, MJD 51893 through 52802. Short runs (less than 4 sub runs) are excluded as well as ADC calibration data and other short low rate runs. The resulting exposure is 834.5 days of data out of 884.2 days, or 91%. The analysis uses two hour direct integration of the background. A cut requiring nFit$>$ 20 PMTs and a gamma-hadron cut of $X2 > 2.5$ are applied. A variety of time checks are applied to get rid of events with bad timestamps, time gaps, etc. The combined cuts retain 5.8% of the events read for analysis. The analysis includes the zenith_align2 pointing correction and the sky maps include the rounding correction introduced by Erik Blaufuss. The data is also corrected for the calibration shift in the PE scale so that the same X2 distribution applies throughout the data set. I have included some additional changes to the background calculation suggested by Gus that bring the total event count in the on and off maps within agreement to less than 1 part in 10^6. The source bin size is 2.1° in declination (δ) by $2.1^\circ/\cos(\delta)$ in right ascension.

I have recently extended the analysis to include data up to this year's repair and to correct for the PE shift in calibration version 406. I have left Tables 4 and 5 with the original numbers as the general nature of the results is unchanged and it takes a bit of time to rerun and redo the tables. Table 6, however, has the 920 day data set numbers so that you can see the most current comparison.

6 Comparing Flux Limits to Predicted Flux

6.1 TeV Spectral Index

To compare Milagro observations with the Costamante and Ghisellini predictions the same spectrum used to calculate the given integral fluxes must be applied to the calculation of flux using Milagro data. The Fossati model is a parameterization using parabolic shapes for the peaks so there is no well-defined power law index. Instead, an index is estimated by requiring a power law spectrum consistent with the integral fluxes above 300 GeV and 1 TeV. The power law estimation is reasonably good because the shape of the SED, particularly for the modifed Fossati model, is fairly linear over a small energy range even near the peak region. This can be seen in the SED shown for Mrk 421 in Figure 1.

The SSC model SED predictions steepen sharply above a few hundred GeV and most of the sample is not predicted to have an appreciable flux

above 1 TeV. Milagro is most sensitive near energies of a few TeV. This means most of the SSC flux predictions are below the level at which Milagro is sensitive. For these reasons the comparison is only made directly for SSC model predictions that extend above 1 TeV. For those objects that have a TeV flux prediction the spectral index is approximated in the same way as for the Fossati model predictions, as a power law consistent with the integral fluxes above 300 GeV and 1 TeV.

6.2 Aside on Some Details of SSC Modeling

This is a brief divergence to summarize my attempts to find an estimate for the spectral shape from SSC model parameters . The motivation for this was a relation between spectral index and the slope of the emitting electron distribution that holds under certain conditions (see [10] for more details). The relation is $\alpha_{TeV} = n - (n-1)/2$, where n is the slope of the emitting particle distribution, $N \propto E^{-n}$. A basic SSC model applies the Thompson cross section to the inverse Compton scattering of synchrotron photons by the emitting electrons. However, in the relativistic limit the Thompson cross section is traded for the Klein-Nishina cross section when $E_{Comp} > m_e c^2/E_{synch}$. The spectrum becomes a power law above the Compton peak in the extreme Klein-Nishina limit (defined as $\gamma_b \nu_s \geq (3/4)mc^2/h$, where γ_b is the Lorentz factor of the electrons at the cooling energy and ν_s is the synchrotron photon frequency.) In this limit the integral over the emissivity is dominated by the component arising from the highest energy electrons and the lowest energy synchrotron photons. While all of the objects in the sample are affected by the Klein-Nishina limit they are not all in the extreme limit and include non-negligible contributions from the other combinations of emitting electrons and synchrotron photon distributions. This means that although the TeV spectrum is very similar to a power law, the slope of the emitting particle distribution alone is not enough to accurately predict the TeV spectral index for the objects in the sample.

7 Results

7.1 Hard and Soft Flux Limits

The TeV spectra are unknown for these sources except for 1ES 1959+650 which has been detected by ACTs. In the absence of a spectral measurement, two extreme power law values are used to calculate flux limits for the sources. AGN observations by ACTs measure spectra ranging from approximately $dN/dE \propto E^{-2.0}$ to $\mathrm{E}^{-3.0}$. This represents approximately the

softest and hardest spectra observed in AGN at TeV energies. Setting upper limits for both gives in some sense an upper and lower bound on the limit. In the context of the flux correlated spectral variability observed in Mrk 421 and 1ES 1959+650, the bounds could be interpreted as flaring and quiescent limits. There is evidence from both objects that the TeV spectral index hardens with increased luminosity. Additionally, within the SSC model TeV and X-ray emission is predicted to be closely correlated and BL Lacs are generally known for X-ray spectra that harden with luminosity. The flux limits are given for each source using power law indexes -2.0 and -3.0 and also with IR attenuation included in Tables 4 and 5. The limits are on the differential flux I_0 at 95% confidence level using the method of Helene [6]. The IR attenuation is calculated using both the baseline model of Stecker and de Jager [9] and the Semi-Analytic Model (SAM) of Primack and Somerville as parameterized by Bullock [2].

7.2 1ES 1959+650

One of the predicted TeV emitters has been detected by ACTs. The outburst in 2002 was detected by HEGRA, CAT, and VERITAS. HEGRA has published fits to low and high state spectral data using two forms, $dN/dE = I_0 E^{-\alpha}$ and $dN/dE = I_0 E^{-\alpha} e^{-E/E_c}$ ([1]). The low state observations are 150 hours of data taken from 2000 to 2002. The high state data is for 6 nights (8.5 hrs) in May and July of 2002 when the flux above 2 TeV exceeded 1 Crab. HEGRA's sensitivity is at slightly higher energies than Milagro and the data set has not been matched to the dates HEGRA was observing so these limits are not directly comparable to the HEGRA measured flux. The Milagro upper limits on the differential flux for several fits to the spectrum of 1ES 1959+650 are in Table 2.

HEGRA Spectral Fit	α	E_c (TeV)	I_o U.L Milagro ($10^{-11} \frac{phot}{cm^2 sTeV}$)
high	2.83	none	0.95
	1.83	4.2	0.85
low	3.18	none	1.36
	1.8	2.7	1.33

Table 2: Milagro flux limits set for 1ES 1959+650 for the 832 day data set for several spectral shapes. The spectral shapes are from HEGRA fits to data taken during both high (> 1 Crab) and low (< 0.5 Crab) flare states [1]. The form of the differential spectrum is $dN/dE = I_o E^{-\alpha} e^{-E/Ec}$.

7.3 Comparison

The Milagro limits can be used to make a comparison with the predicted fluxes from Costamante and Ghisellini [4] and in some cases constrain the model prediction. The predicted fluxes are given in integral form, but the differential flux is a more straightforward interpretation of Milagro data. This is because Milagro does not have a sharp low energy cut off. To make a direct comparison the Costamante and Ghisellini results are converted to differential form using the power law approximation to the spectrum already discussed. Using the power law approximation the differential flux is unfolded from the integral fluxes above 300 GeV and 1 TeV. The approximation applies above 300 GeV where Milagro has most sensitivity. The approximation is only possible for predictions with a significant amount of flux above 1 TeV. For this reason the comparison is not made for most of the SSC model predictions. The calculated Milagro fluxes are listed for the predicted model spectra with the recalculated predicted fluxes in Table 6. These limits have been updated to reflect the 920 day data set.

Note: If the comparison is made instead for the given predicted integral flux and the Milagro differential flux integrated over the estimated spectrum, the relative results are not much changed.
Additional Note: There is not a clearly defined way to publish these limits or to make the comparison to the predicted fluxes even though the predictions were published in a form inteneded for ACTs. VERITAS is publishing their limits on some of these objects in two papers that compare in two slightly different ways: in integral flux units with the integral flux scaled to > 300 *GeV and in Crab units which requires the conversion of the predictions to the same. My conclusion is that converting the Costamante predictions to differential form is fine as long as it is clearly described.*

The predicted fluxes can be put into perspective by figures 3 and 4. The figures give sensitivity using the differential flux I_0 necessary for a 3σ observation as a function of redshift and declination for two spectral indexes. Sources with a flux prediction near this level are likely to be constrained in the data set. For example, for the modified Fossati model 1ES0033+595 at $\delta = 60$ has a prediction of 6.03 (in $10^{-12} phot/cm^2 sTeV$) and the 3σ I_0 at z=0 for $\alpha = 2.0$ is ≈ 5. It is constrained at 4.69 without IR attenuation included. At z=0.086 $I_0 \approx 80$ for a 3 sigma observation. The ratio of the predicted flux to the detectable flux gives a sense of how much additional exposure is necessary to constrain the prediction. The exposure time scales by the square root of this ratio, $t_{detect} = \sqrt{3\sigma I_0 / I_{pred}} * 920.46$ days. A more optimistic example is RGB 0214+517 at z=0.049 and $\delta = 51.7$. When the the limit is redshift corrected I_0 goes to 20.5 which is not far from

constraining the modified Fossati prediction at 17.6 even with IR included. For this source the 3σ flux is about 20 so the IR adjusted limit should constrain the model in a few months ($\sqrt{}(20/17.6) = 1.07$, $1.07 * 920.5 = 984$ days total exposure.) It is also useful to note that the observations are in the gaussian regime so the given 3σ I_0 can be scaled to change the significance level. For example, the 5σ I_0 is approximately $5/3^* I_0$.

8 Conclusion

In this memo soft and hard spectral limits are set for a set of possible TeV blazars and the effects of changes in the spectral shape on the limits are described. This set of TeV limits for the BL Lacs selected by Costamante and Ghisellini is one of the more complete since some of the sources are predicted to be too far away or too faint to merit observations by the current ACTs. The predicted SEDs for the sources are used to compare the predicted flux with Milagro upper limits. None of the limits constrains any of the SSC model predictions. Table 3 notes the eight sources with Fossati style predictions that are constrained by the Milagro limits as well as those constrained by other detectors. Two of the BL Lacs, 1ES 0806+524 and RGB 1117+202 are quite close to being constrained in the data set presented here and by estimation will be in about another 6 months of data.

None of the SSC model fluxes are at the level that can be expected to be constrained. The fluxes given are at most $0.7\text{x}10^{-12}$ which requires about 3.7 times the current exposure using the $\alpha = 3$ plot and that is without IR attenuation considered.

The fluxes that Milagro constrains can be interpreted two ways: loss due to IR attenuation of the source spectrum or over prediction by the Fossati style model.It is interesting to ask whether any of the objects are still constrained when attenuation effects are included in the spectrum. This has the effect raising the Milagro limits as described in the flux discussion and demonstrated by Figure 2. No changes are made to the model fluxes because they are converted into differential form so the effects of attenuation are in the spectral shape and are separated from the differential flux factor, I_0. The predictions for I ZW 187 and RGB 1725+118 are still constrained after the IR attenuation is included. However, keep in mind that RGB 1725+118 has a somewhat dubious redshift measurement making the IR correction uncertain.

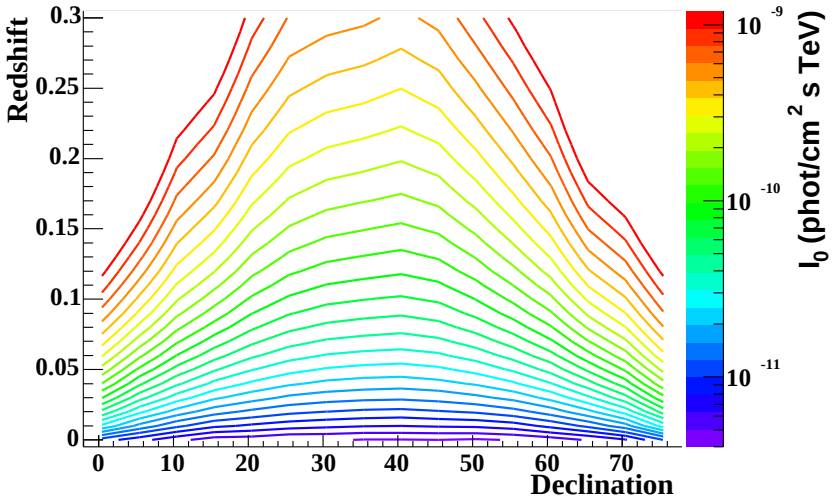

Figure 3: Differential flux , I_0 of $dN/dE = I_0(E/TeV)^{-\alpha}e^{-\tau(E,z)}$ with $\alpha = 2.0$, necessary for a three sigma observation of a source at the given declination and redshift in 920.46 days. The redshift attenuation is obtained using the baseline model of Stecker and de Jager [9].

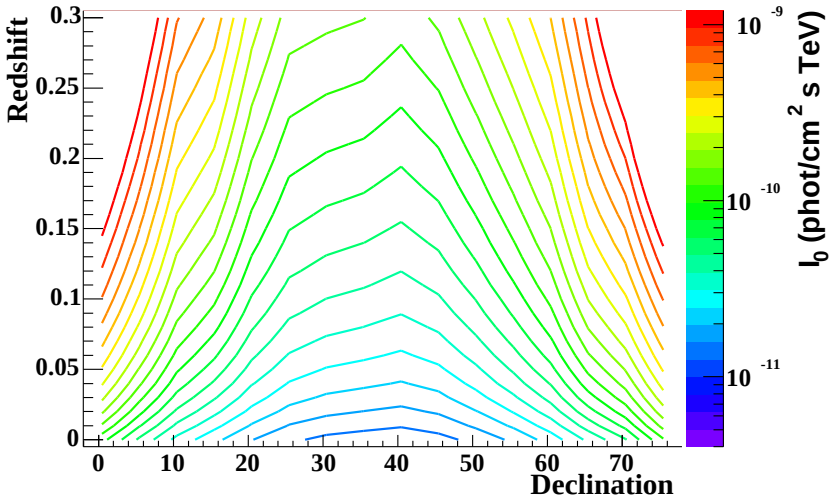

Figure 4: Same as Figure 3 with $\alpha = 3.0$

References

[Aharonian et al.(1999)] Aharonian, F. A. et al. 1999, A&A, 349, 11

[Aharonian et al.(2002)] Aharonian, F. et al. 2002, A&A, 393, 89

[1] Aharonian, F. et al. 2003, A&A, 406, L9

[2] Bullock, J 1999, Ph.D. Thesis

[3] de la Calle Perez, I. 2003, ApJ, in press (astro-ph 0309063)

[4] Costamante, L., Ghisellini, G. 2002, A&A, 384, 56

[5] Fossati G., et al. 1998, MNRAS, 299, 433

[6] Helene, O. 1983, NIM, 212, 319

[7] Holder, J. 2003, ApJ, 583, L9

[8] Horan, D. et al. 2003, ApJ, in press (astro-ph 0311397)

[Krennrich et al.(1999)] Krennrich, F. et al. 1999, ApJ, 511, 149

[Samuelson et al.(1998)] Samuelson, F. W. et al. 1998, ApJ, 501, L17

[9] de Jager, O., Stecker F. 2002, ApJ, 566, 738

[10] Tavecchio, F., Maraschi, L., Ghisellini, G. 1998, ApJ, 509, 608

Name	RA	DEC	z	α_1	α_2
1ES 0033+595	8.97	59.83	0.086	2.16	2.50
1ES 0120+340	20.78	34.35	0.272	2.25	–
RGB 0136+391	24.14	39.10	0.2*	2.25	4.28
RGB 0214+517	33.57	51.74	0.049	2.14	3.01
3C 66A	35.67	43.04	0.444	3.19	–
1ES 0229+200	38.20	20.29	0.139	2.23	4.62
1H 0323+022	51.56	2.42	0.147	2.25	–
1H 0414+009	64.22	1.09	0.287	2.43	–
1ES 0647+250	102.69	25.05	0.2*	2.29	–
1ES 0806+524	122.45	52.32	0.138	2.31	–
RGB 0812+026	123.00	2.63	0.2*	2.28	–
OJ 287	133.70	20.11	0.306	3.19	–
1H 1013+498	153.77	49.43	0.200	2.47	–
1ES 1028+511	157.83	50.89	0.361	2.62	–
RGB 1117+202	169.28	20.24	0.139	2.15	–
MRK 180	174.11	70.16	0.045	2.19	–
RGB 1136+676	174.12	67.62	0.135	2.19	–
ON 325	184.47	30.12	0.237	2.72	–
1H 1219+301	185.34	30.18	0.182	2.21	–
RGB 1417+257	214.49	25.72	0.237	2.26	–
1ES 1440+122	220.70	12.01	0.162	2.10	2.82
1ES 1553+113	238.93	11.19	0.360	2.91	–
RGB 1725+118	261.27	11.87	0.018	2.10	3.25
I Zw 187	262.08	50.22	0.055	2.15	–
1ES 1741+196	265.99	19.59	0.084	2.17	3.80
1ES 1959+650	300.00	65.15	0.047	2.17	–
BL Lacertae	330.68	42.28	0.069	2.69	–

Table 3: BL Lacs selected as likely TeV emitters by Costamante and Ghisellini that are within the field of view of Milagro. The Fossati parameterization, α_1, and SSC model fit, α_2, to the energy spectrum are approximated as power laws above 100 GeV where possible.
*: unknown z set to be 0.2.

Object	z	I_0 (E_{med}) $[\frac{10^{-11}}{cm^2 sTeV}]$	I_0 IR1 (E_{med})	I_0 IR2
1ES 0033+595	0.086	0.31 (11.8)	7.53 (1.2)	4.39
		1.51 (2.0)	6.18 (0.48)	6.03
1ES 0120+340	0.272	0.36 (7.6)	36.10 (0.32)	37.7
		1.03 (1.3)	9.39 (0.21)	10.1
RGB 0136+391	0.200	0.29 (7.6)	15.50 (0.40)	9.29
		0.83 (1.2)	5.13 (0.26)	3.30
RGB 0214+517	0.049	0.25 (9.1)	1.80 (1.91)	1.20
		0.93 (1.5)	2.12 (0.63)	2.07
3C 66A	0.444	0.31 (7.6)	105.00 (1.26)	128
		0.90 (1.9)	19.60 (0.16)	24.1
1ES 0229+200	0.139	0.44 (8.5)	16.90 (1.55)	13.3
		1.57 (0.6)	8.15 (0.35)	8.85
1H 0323+022	0.147	0.69 (18.6)	100.00 (0.65)	46.5
		5.64 (3.8)	59.30 (0.51)	45.5
1H 0414+009	0.287	0.67 (25.1)	736.00 (0.34)	606
		6.54 (3.9)	253.00 (0.29)	223
1ES 0647+250	0.200	0.19 (7.8)	12.00 (0.41)	10.9
		0.61 (1.3)	3.90 (0.26)	3.82
1ES 0806+524	0.138	0.29 (9.1)	11.30 (0.62)	6.98
		1.05 (1.5)	5.56 (0.35)	4.78
RGB 0812+026	0.200	0.46 (17.0)	152.00 (0.54)	107
		3.79 (3.4)	68.80 (0.40)	61.7
OJ 287	0.306	0.32 (8.5)	65.10 (0.30)	73.6
		1.15 (1.5)	16.30 (0.20)	18.4
1H 1013+498	0.200	0.54 (7.9)	38.50 (0.42)	16.6
		1.84 (1.5)	13.30 (0.28)	6.29

Table 4: The 95% c.l. upper limits on I_0, where $dN/dE = I_0(E/TeV)^{-\alpha}e^{-\tau(E,z)}$. The differential flux is quoted at the median triggered energy which depends on the spectral shape and the source declination. For each AGN the first row gives limits for $\alpha = 2.0$ and the second for $\alpha = 3.0$. IR1 indicates the baseline evolution IR background model of de Jager and STecker [9] and IR2 indicates the semi-analytic model of Primack and Somerville as parameterized by Bullock [2]. The IR2 flux limits have been interpolated because the parameterization is course in redshift. The median energies are not listed for this reason.

Object	z	I_0 (E_{med}) $[\frac{10^{-12}}{cm^2 sTeV}]$	I_0 IR1 (E_{med})	I_0 IR2
1ES 1028+511	0.361	0.25 (8.5)	82.50 (0.26)	54.1
		0.90 (1.5)	18.90 (0.19)	12.6
RGB 1117+202	0.139	0.45 (8.5)	17.50 (0.63)	8.36
		1.63 (1.5)	8.47 (0.35)	5.57
Mrk 180	0.045	0.37 (17.8)	5.04 (3.16)	2.1
		2.90 (3.1)	8.62 (0.76)	6.2
RGB 1136+676	0.135	0.55 (17.0)	65.60 (0.68)	28.1
		4.20 (3.4)	36.40 (0.43)	27.6
ON 325	0.237	0.47 (7.4)	36.70 (0.35)	30.0
		1.37 (1.3)	10.80 (0.23)	9.36
1H 1219+301	0.182	0.59 (7.4)	27.40 (0.46)	20.6
		1.72 (1.3)	9.94 (0.28)	8.59
RGB 1417+257	0.237	0.51 (7.6)	46.50 (0.35)	47.7
		1.63 (1.3)	13.60 (0.22)	14.9
1ES 1440+122	0.162	0.39 (11.2)	34.80 (0.56)	17.0
		1.96 (2.1)	15.80 (0.34)	10.9
1ES 1553+113	0.360	0.38 (11.2)	206.00 (0.23)	159
		1.86 (2.1)	49.80 (0.21)	39.3
RGB 1725+118	0.018	0.60 (11.2)	1.70 (5.50)	1.24
		2.97 (2.1)	4.56 (1.35)	4.07
I Zw 187	0.055	0.16 (8.3)	1.28 (1.74)	0.63
		0.56 (1.5)	1.34 (0.60)	0.96
1ES 1741+196	0.084	0.58 (8.5)	9.07 (1.10)	4.76
		2.07 (1.5)	6.83 (0.49)	5.35
1ES 1959+650	0.047	0.32 (12.9)	3.57 (3.24)	1.05
		2.01 (2.9)	6.00 (0.79)	2.91
BL Lacertae	0.069	0.34 (7.4)	3.11 (1.23)	1.71
		0.98 (1.3)	2.45 (0.49)	1.92

Table 5: 95% c.l. upper limits continued.

Object	z	α	I_0 U.L.	I_0 U.L. with IR	Predicted I_0
1ES 0033+595[a,5]	0.086	2.16 / 2.50	4.69 / 8.82	81.2 / 79.8	6.03 / 0.649
1ES 0120+340[4]	0.272	2.25 / –	5.05 / –	246 / –	0.81 / 0.790
RGB 0136+391	0.200	2.25 / 4.28	2.56 / 2.28	70.2 / 4.3	1.62 / 0.104
RGB 0214+517[a,5]	0.049	2.14 / 3.01	3.52 / 9.87	20.5 / 22.2	17.63 / 0.137
3C 66A[1,4]	0.444	3.19 / –	9.75 / –	149 / –	0.24 / –
1ES 0229+200[1,4]	0.139	2.23 / 4.62	7.25 / 6.59	160 / 9.66	2.79 / 0.174
1H 0323+022[1,4]	0.147	2.25 / –	10.3 / –	699 / –	2.42 / 0.014
1H 0414+009[1]	0.287	2.43 / –	16.1 / –	3500 / –	0.62 / 0.133
1ES 0647+250[1]	0.200	2.29 / –	2.82 / –	79.6 / –	1.67 / 0.504
1ES 0806+524[5]	0.138	2.31 / –	4.31 / –	81.3 / –	3.82 / –
RGB 0812+026	0.200	2.28 / –	7.70 / –	998 / –	1.66 / 0.074
OJ 287[2]	0.306	3.19 / –	11.7 / –	116 / –	0.73 / –
1H 1013+498	0.200	2.47 / –	4.97 / –	104 / –	0.32 / 0.336
1ES 1028+511[4]	0.361	2.62 / –	3.81 / –	195 / –	1.05 / –
RGB 1117+202[4]	0.139	2.15 / –	3.95 / –	105 / –	3.48 / 0.157
Mrk 180[a,1,2,5]	0.045	2.19 / –	5.27 / –	51.3 / –	24.91 / 0.050
RGB 1136+676	0.135	2.19 / –	7.25 / –	489 / –	2.70 / 0.183
ON 325[4]	0.237	2.72 / –	9.16 / –	121 / –	0.37 / –
1H 1219+301[1,4]	0.182	2.21 / –	6.76 / –	183 / –	1.96 / 0.336
RGB 1417+257	0.237	2.26 / –	7.89 / –	339 / –	1.09 / 0.455
1ES 1440+122	0.162	2.10 / 2.82	3.33 / 11.1	221 / 127	2.35 / 0.198
1ES 1553+113[2,4]	0.360	2.91 / –	11.6 / –	382 / –	0.42 / 0.777
RGB 1725+118[a,5]	0.018	2.10 / 3.25	7.19 / 33.0	18.8 / 45.6	39.03 / 0.025
I Zw 187[a,1,5]	0.055	2.15 / –	1.66 / –	10.5 / –	15.39 / 0.145
1ES 1741+196[a,1,5]	0.084	2.17 / 3.80	6.55 / 15.4	74.2 / 26.2	10.61 / 0.319
1ES 1959+650[a,b]	0.047	2.17 / –	2.77 / –	24.2 / 28.9	21.99 / 0.051
BL Lacertae[a,1,5]	0.069	2.69 / –	6.88 / –	23.6 / 25.5	7.87 / 0.173

Table 6: Comparison of differential flux 95% c.l. upper limits with predicted fluxes converted to differential form. The assumed spectrum is $dN/dE = I_0(E/TeV)^{-\alpha}$, where I_0 is in 10^{-12} phot/cm^2 s TeV. The limits are given for two spectra. The first alpha is the estimated power law index for the modified Fossati SED model. The second is for the SSC model. Limits are also given with IR attenuation included using $dN/dE = I_0(E/TeV)^{-\alpha}e^{\tau(E,z)}$ where τ is determined using the baseline model of Stecker and de Jager [9].

[a] Flux limit falls below predicted flux. [b] TeV detection by ACTs [7]. [1] TeV limit in [4]. [2] Predicted flux constrained by ACT TeV limit [4]. [4] TeV limit from VERITAS [8], [3]. [5] Constraining TeV limit from VERITAS [8], [3].